Influence of precursor crystallinity on photocatalytic activity of PdS/CdS-ZnS

P. SVERA[a,b], A.V. RACU[a,c], C. MOSOARCA[a], D. URSU[a,b], P. A. LINUL[a], R. BAIES[a,b], R. BANICA[a,b*]

[a]National Institute for Research and Development in Electrochemistry and Condensed Matter, 1 Plautius Andronescu Str, 300224 Timisoara, Romania
[b]University Politehnica Timisoara, Piata Victoriei 2, 300006 Timisoara, Romania
[c]Institute of Applied Physics of Moldova, ASM, Academiei str 5, Chisinau, Moldova

In this work we present the synthesis and the photocatalytic activity of PdS/CdS-ZnS composites. The photocatalysts were obtained in hydrothermal conditions at 170 ºC from zinc sulphides as sulphide source. The products were characterized by powder X-ray diffraction scanning electron microscopy, energy-dispersive X-ray, transmission electron microscopy, UV–visible and photoluminescence spectroscopies. From Tauc plot the optical energy gap was found to be nearly 2.40 eV. Experiments for hydrogen evolution were conducted in sulfide/sulfite aqueous solution under visible light. The size of photocatalyst nanoparticles and the efficiency of water splitting reaction increases with increasing of ZnS precursor crystallinity. The maximum value for hydrogen evolution rate is 3.8 mmol·g^{-1}h^{-1}, for the sample with the highest crystallinity.

1. Introduction

The demand for energy sources that will substitute oil and environmental cleanness makes hydrogen production by photocatalytic water splitting a promising area of research [1-4]. Nowadays technological interest is focused on photocatalysts with ability to absorb light in visible region, which accounts for about 43 % of the solar spectrum [1,5]. For photocatalytic water splitting reaction, such materials must be able to: absorb light for generating electron-hole pairs, to have an appropriate surface where charge separation and reactions of water reduction or oxidation takes place [6]. Metal sulfides materials such as $CuInS_2$ [7], CdS [8], $ZnIn_2S_4$ [9] are promising photocatalysts due to their suitable band gap and good catalytic activities for H_2 production [2,10,11]. Also zinc sulphide (ZnS) compounds have high photocatalytic activity because of the rapid generation of electron-hole pairs by incident photon and the highly negative potential of excited electrons in the conduction band [2,12-14]. But its wide band gap makes it useless for visible light pumping. A common way for shifting ZnS's wide band gap energy (3.35 eV) to visible region is by doping with Cu [15], Cd [16], or In [17] or using dual/coupled systems such as ZnS-CdS, ZnS-CuS, $ZnS-WS_2$ [2,18] composites. These compounds show great ability to produce hydrogen from water splitting as compared to their constituent sulfides. For dual semiconductor photocatalysts the charge

separation mechanism consists in the injection of electrons emerging from photogeneration from one of the semiconductors into the conduction band of the other one [4,11,19,20]. Another interesting way to improve photocatalic activity is thermal treatment of sulfide precursors which greatly increases the H_2-production rate due to the improved crystallinity [2,18]. Wang et al [21] show the products of two–step synthesis of ZnO–CdS core–shell nanorods, with RuO_2 as co-catalyst by SEM and TEM images. They obtained a hydrogen evolution efficiency of 6.18 mmol·g^{-1}h^{-1} in the presence of S^{2-} and SO_3^{2-} as sacrificial reagents under simulated solar irradiation. CdS nanoparticles were synthesized by the following methods: solvothermal synthesis [21], chemical bath deposition [22], ultrasonic irradiation [23], chemical bath dip coating deposition [24].

In this context the aim of our study, was to compare the photocatalytic efficiency of two PdS/CdS-ZnS composites compounds obtained from uncrystallized and crystallized ZnS precursors.

2. Experimental

2.1. Materials

Sodium sulfide nonahydrate ($Na_2S \cdot 9H_2O$), zinc sulfate heptahydrate ($ZnSO_4 \cdot 7H_2O$), glacial acetic acid

($C_2H_4O_2$), sodium sulfite (Na_2SO_3), cadmium nitrate tetrahydrate ($Cd(NO_3)_2 \cdot 4H_2O$), palladium(II) chloride ($PdCl_2$) were of analytical grade and purchased from Sigma Aldrich. Bi-distilled water was used in all experiments.

2.2. Sulfur source synthesis

For the PdS/CdS-ZnS photocatalysts preparation, two types of precursors were used:

i) ZnS obtained by precipitation of Zn^{2+} ions with Na_2S (ZnS_{PP}) and; ii) ZnS obtained by precipitation (as in the previous case) and subsequently, hydrothermally crystallized (ZnS_{CR}) at 200 °C. As a result of this treatment, cubic crystallized ZnS was obtained.

Sulfur source synthesis was made by precipitation as follows: 192, 14 g of $Na_2S \cdot 9H_2O$ were dissolved in 200 mL distilled water. Separately, 57,5 g of $ZnSO_4 \cdot 7H_2O$ were dissolved in 140 mL distilled water. Previously prepared zinc sulfate was added under stirring, resulting in instant ZnS precipitation. The mixture was then cooled under water bellow 20 °C. The resulted suspension was centrifuged at 5000 rot/min. One half of the solid was dried under vacuum at 65 °C for eight hours (ZnS_{PP}) and the other half was exposed to hydrothermal treatment at 200 °C for 20 hours (ZnS_{CR}). After hydrothermal treatment, the ZnS_{CR} was washed with distilled water and dried in the same conditions as ZnS_{PP}.

2.3. Photocatalyst synthesis

The procedure consists in suspension the ZnS precursor (283 mg ZnS_{CR} or 291,3 mg ZnS_{PP}) in 30 mL of water under ultrasonication for 30 minutes. Afterwards, 1 mL of glacial acetic acid was added under stirring. After 5 minutes, 4 mL of $PdCl_2$ was added to the suspension. The rapid change in color, from white to light brown, shows the interaction between Pd^{2+} and ZnS with formation of PdS. After 2 minutes 35 mL of 0.057 M cadmium nitrate solution was added. The mixture was hydrothermally treated for 20h (P1 and P2) and 40h (P3) at 170 °C. The cooling took place naturally at room temperature. The obtained precipitates were centrifuged and washed with distilled water. The final products were dried in vacuum at 65 °C for 4 hours.

2.4. Characterization

The X-ray diffraction (XRD) patterns were collected by an X'Pert Pro MPD diffractometer using $Cu_{K\alpha}$ radiation. The morphologies were studied using a scanning electron microscope (SEM) - FEI Inspect S and a transmission electron microscope (TEM) - Titan G2 80-200. The elemental analysis of CdS/ZnS composite materials was performed by energy-dispersive X-ray (EDX) - FEI Inspect S. Reflectance spectra for as obtained material were collected using a UV-VIS spectrometer - Lambda 950 - PerkinElmer. The photoluminescence (PL) spectra were recorded on a fluorescence spectrometer - FLS 980, Edinburgh Instruments.

2.5. Photocatalytic hydrogen evolution

The photocatalytic performance for the synthesized materials was investigated in a closed system. For this, 50.0 mg of photocatalyst was dispersed in 250 mL 0.2 M $Na_2S \cdot 9H_2O$ and 0.1 M Na_2SO_3 aqueous solution. The suspension was irradiated by a 150 W Xenon lamp (Osram) equipped with an optical cut-off filter (λ=400 nm – Thorlabs Inc.). The Pyrex-photoreactor provided with water jacket, was maintained at constant temperature 298±1 K using thermostated water bath. The catalyst was continuously stirred to keep a homogenous suspension. Before starting the photocatalytic process, nitrogen 4.6 (LindeGaz Romania) was purged trough the reactor to remove the air from system. The rate of H_2 evolution was determined by measuring the dislocated water volume in a 100 mL burette. The photocatalytic activity was monitored and recorded for 24 h.

3. Results and discussion

3.1. Chemical aspects

The synthesis of CdS based photocatalysts using ZnS as a S^{2-} ion source is based on ZnS lower solubility than the one exhibited by the CdS. However, the K_{sp} values of the two compounds (i.e ZnS si CdS) at room temperature are not so different from each other (cca. 10^{-23} mol^2/L^2 for β-ZnS vs cca. 10^{-27} mol^2/L^2 for CdS). The solubility difference makes the exchange between Zn^{2+} and Cd^{2+} ions to take place slowly. The main reactions for the photocatalysts synthesis are:

$$ZnS + Cd^{2+} \rightarrow CdS + Zn^{2+}$$
$$ZnS + xCd^{2+} \rightarrow Zn_{1-x}Cd_xS + xZn^{2+}$$
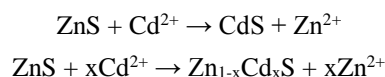
The reaction rate between zinc sulfide and cadmium ions increases with the increasing of temperature and with the decreasing of ZnS particle sizes. For this reason ZnS_{PP} will react with higher rate than ZnS_{CR}.

It is generally accepted that in order to achieve high efficiency photocatalysts is necessary to obtain powders with high specific surface area to increase the density of

the active centers and high crystallinity to reduce the recombination process which is competing with the chemical reactions.

3.2. Crystal structure characterization

X-ray diffraction patterns for samples (Fig. 1) obtained using ZnS_{CR} respectively ZnS_{PP} (at 2 different reaction times), highlight the major differences between the reaction products. Rietveld analysis shows in the case of ZnS_{CR} precursor, the existence of an $Zn_{1-x}Cd_xS$ hexagonal - type compound, as a majority crystalline phase (83.3 %), with the unit cell having V=99.12 nm^3 (a=4.13031 and c=6.70911) very close to the pure CdS, together with cubic ZnS (16.7 %) with V=158,292 nm^3 (a=5.40945), which is the unreacted precursor. When using ZnS_{PP}, after 40 h reaction time, the existence of $Zn_{1-x}Cd_xS$ hexagonal phase (70 %), where the unit cell volume was 98,178 (a=4.11685 and c=6.68890) and cubic phase $Zn_{1-x}Cd_xS$ (30%), having V=195,680 nm^3 and a=5.80562 nm, were evidenced. The average grain size, calculated with the Scherrer equation, for the hexagonal phase obtained after a reaction time of 40 h (P3) was only 12 nm and 57 nm for the P1 sample. Thus the $Zn_{1-x}Cd_xS$ hex. grain growth, through a recrystallization process, is less important at 200ºC. On the contrary, the slow sulfide ions release in the solution results in a lower density of nucleation centers with the formation of larger crystals.
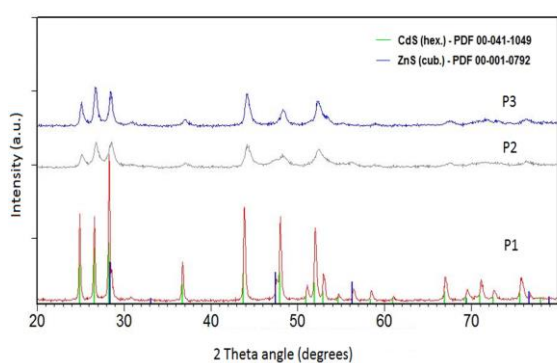

Fig. 1. XRD spectra of P1, P2 and P3 sample obtained by hydrothermal synthesis at 170ºC

TEM and SEM images for P1 and P2 samples highlight the well-defined crystallites with dimensions between 30 and 300 nm in the case of P1 sample (Fig. 2 a) and between 10 and 20 nm for P2 sample (Fig. 2 c). Some larger particles can still be seen in this sample. HRTEM images highlight the existence of CdS/ZnS heterojunctions, which can improve the photocatalytic efficiency (Fig. 2 b).

EDX global spectrum (Fig. 3) for the sample obtained from ZnS_{CR} highlight an atomic ratio of Zn:Cd:S 1:4.3:5.5. The Cd:Zn atomic ratio of 4.3, obtained from the EDX analysis is higher than the one obtained from the semi-quantitative XRD analysis (about 4.98), considering the sample an hexagonal CdS and cubic ZnS mixture.

Higher values of zinc content obtained from the EDX analysis are attributed to the fact that a small proportion of zinc exist in the form of $Zn_{1-x}Cd_xS$ solid solution in which the x value is close to 1. In the case of samples obtained from ZnS_{PP}, the compositional analysis highlights a Zn:Cd:S ratio of 1:2.2:3.2 (20 hours reaction time) and of 1:7.3:8.4 (40 hours reaction time), which proves the fact that, in the solid solution, the cadmium quantity is growing with the increase of the reaction time. The samples traces of oxygen and carbon, in all cases, can be assigned to the superficial oxidation during handling and acetate ion adsorption on the surface of the photocatalyst.
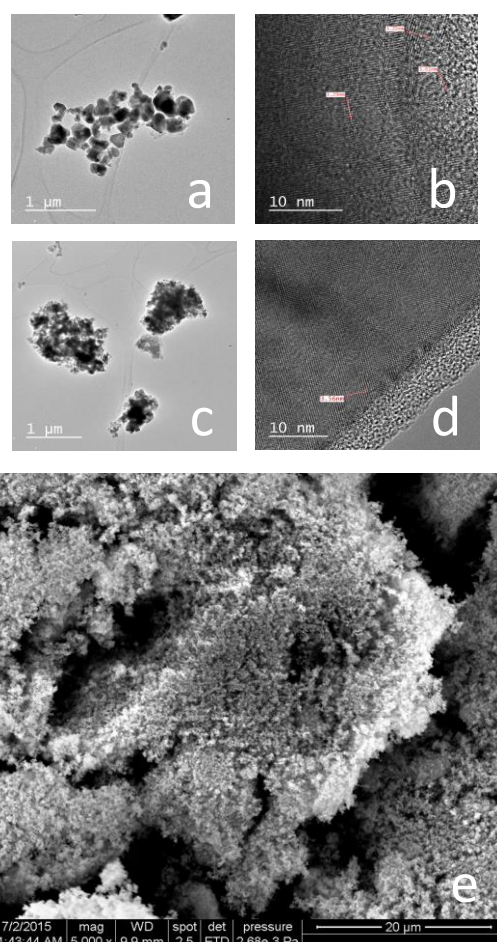

Fig. 2. TEM and SEM images of photocatalysts obtained from different ZnS precursors: a, b, e- P1 and c, d - P2

To verify the existence of two distinct phases for P1 sample, one very rich in CdS hex. and the other consisting

of cubic ZnS, compositional maps, based on the characteristic X - ray radiation were done.

These maps bring out clearly the existence of ZnS/CdS heterojunctions (Fig. 4). Also some "islands" having high concentration of Pd can be seen on the surface of CdS crystallite highlighting the PdS presence on the photocatalyst surface. The compositional map also shows that a large quantity of Pd^{2+} is equally distributed inside the photocatalyst or on its surface. In the case of P2 sample, a much larger homogenity of element distribution can be observed. However some areas richer in Zn^{2+} and poorer in Cd^{2+} can be seen. Homogeneous areas are assigned to the solid solution formed between ZnS and CdS. Inhomogeneous areas richer in Zn^{2+} and Cd^{2+} are assigned to the CdS cubic phase and ZnS cubic unreacted respectively. For the P2 sample, traces of cubic ZnS can be observed in the XRD pattern. This phase disappear with the increase of the reaction time at 40 hours, confirmed by the EDX overall data, which highlights the enriching in CdS of the compound. In this case, also, the existence of islands composed of PdS can be seen clearly. Due to the low PdS concentration, this phase cannot be observed in the XRD spectra.
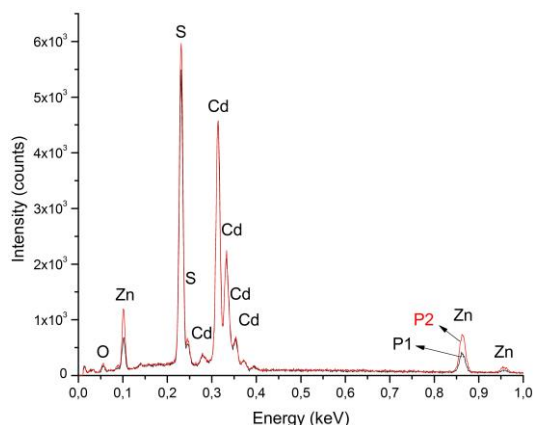

Fig. 3. EDX spectra for P1 and P2

3.3. Optical characterization

Two comparative reflectance spectra of the photocatalysts samples were obtained for P1 and P3 respectively. As shown in Fig. 5, the powders reflectance spectrum, at wavelengths higher than 600 nm, can be a measure of photocatalyst coverage with the cocatalyst (PdS). Less than 30% of incident photons with energy higher than 2.4 eV produce hole-electron pairs in CdS. Most of the remaining photons are partly absorbed by PdS from the broadband semiconductor surface and the other part is involved in excitation processes induced by
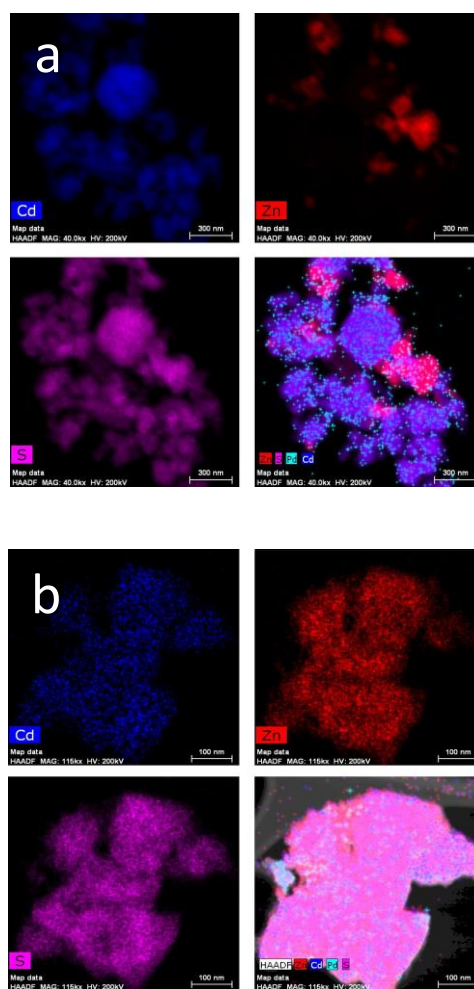

Fig. 4. EDX maps for P1 a) and P2 b) samples

the Pd^{2+} impurities from the CdS crystal lattice. The UV-vis diffuse reflectance measurement has been performed in the range between 380 and 800 nm. From the reflectance spectra depicted in Fig. 5 clearly results that both photocstalysts can absorb well at wavelengths shorter than ~500 nm, whereas for longer wavelengths the reflectivity increases considerably.

The energy gap was calculated based on diffuse reflection spectra (Fig. 5 - inset) using Tauc plot and was found to be nearly 2.40 eV. The absorption coefficient (α) is related to the band gap energy (Eg) as shown in the equation [25-27]:

$$\alpha_{K-M} h\upsilon = A(h\upsilon - Eg)^{1/2}$$

where A is a proportionality constant and $h\upsilon$ is the photon energy According to literature, the error bars for band gap of P1 and P3 samples is estimated to be $\pm$ 0.10 eV [28].

The PL spectroscopy is an effective technique to investigate the photo-generated charge transfer recombination process, defects and impurities which may give an important information for photocatalytic experiments [10]. PL spectra of obtained PdS/ZnS-CdS composites (Fig. 6) were investigated under 340 nm excitation wavelength.
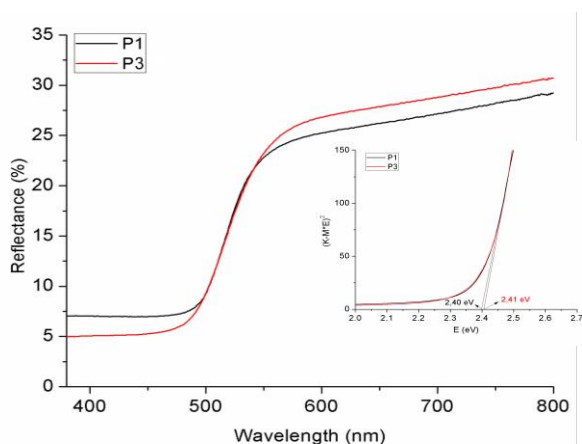
Fig.

5. Diffuse reflection spectra of samples P1, P3

and bandgap estimation (inset)

Few emission peaks between 470-650 nm were detected. Low intensity peaks between 470-525 nm correspond to interband CdS recombination. The most relevant emission has a peak at 582 nm and the intensity of this peak changes as a function of the cubic ZnS content in the samples P1, P2 and P3. It was observed that the peak at 582 nm has a better shape in the case of P1. According to the literature, this peak corresponds to intrinsic ZnS defects related to sulfur vacancy which usually appears for samples prepared at elevated temperature [29, 30].
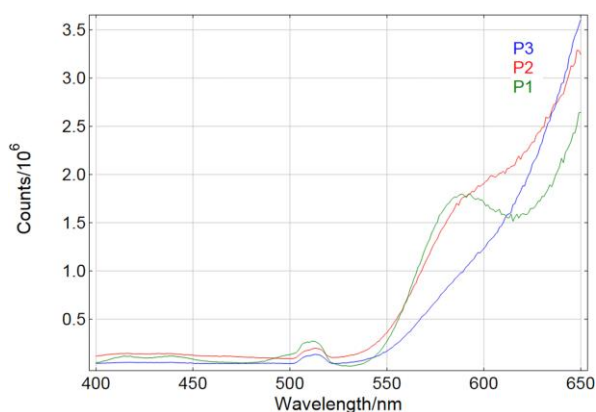

Fig. 6. Photoluminescence spectra of P1, P2 and P3 samples

It is known that suppressing the recombination of photo-excited electron-hole pairs the photocatalytic activity increases [12]. The broad shoulder which begins from 600 nm and lay to more than 650 nm, can be attributed to CdS trap-related states that generally serve as recombination centers.

3.4. Photocatalysis

The photocatalytic H_2 evolution using aqueous solutions of Na_2S and Na_2SO_3 can be represented by the following equations [12, 24]:

$$Metal\ sulfide + h\nu \rightarrow h^+ + e^-\ (\lambda > 400\ nm)$$
$$2H_2O + 2e^- \rightarrow H_2 + 2OH^-$$
$$S^{2-} + 2h^+ \rightarrow S^0$$
$$S^0 + SO_3^{2-} \rightarrow S_2O_3^{2-}$$
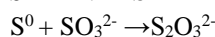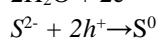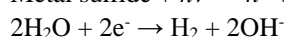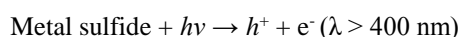
The hydrogen evolution rate determined after 24 h of photocatalysis, was 3.80, 2.86, 2.46 mmolg^{-1}h^{-1} for P1, P2 and P3 respectively (Fig. 7). For the calculation of the error bars of hydrogen evolution rate, it has considered the gas temperature from burette that varies no more than ± 5 °C around 25 degrees while the reactor temperature is constant and the accuracy of the burette which is 0.1.
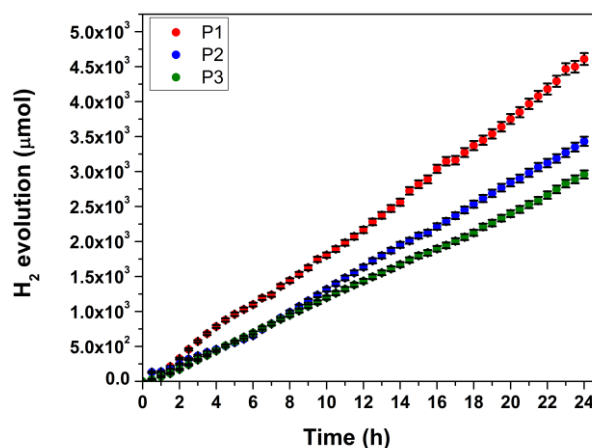

Fig. 7. Hydrogen evolution for P1, P2 and P3 photocatalysts

Therefore hydrogen release yield decreases with decreasing of zinc content and increases with photocatalyst crystallinity. In this case the P2 and P3 high specific surface is less important for the increase of the photocatalyst efficiency than crystallinity of P1 sample.

Probably the recombination process due to the impurity levels is much more important than the band-to-band recombination and plays an important role in reducing the photocatalyst efficiency. Radiative recombination processes due to the sulfur vacancies present in the ZnS crystallites have less influence on the

photocatalyst efficiency. Reducing the number of structural defects by slow release of sulfide ions in the system represents, in our case, the main measure for increasing photocatalyst efficiency.

4. Conclusions

The sulfur source used in the hydrothermal treatment is strongly influencing the crystallinity of the reaction product. $Zn_{1-x}Cd_xS$ (hex) is formed by reactive dissolution of ZnS (cub). The PL spectrum is a good indicator for ZnS (cub) sample content. At approximately same Eg value (2.4 eV), for P1 and P3 samples, the hydrogen evolution rate increases with the increase of the reaction product crystallinity. For P1 sample the hydrogen evolution rate is 3.8 mmol·g^{-1}h^{-1}, for P2 sample is 2.86 mmol·g^{-1}h^{-1}, and for P3 sample 2.46 mmol·g^{-1}h^{-1}.

Acknowledgements

References

[1] Z. Xiong, M. Zheng, C. Zhu, B. Zhang, L. Ma, W. Shen, Nanoscale Res. Lett. **334**, 1 (2013).

[2] E. Hong, D. Kim, J. H. Kim, J. Ind. Eng. Chem. **20,** 3869 (2014).

[3] L. A. Silva, S. Y. Ryu, J. Choi, W. Choi, M. R. Hoffmann, J. Phys. Chem. C **112,** 12069 (2008).

[4] C. H. Liao, C.W. Huang, J.C.S. Wu, Catalysts **2**, 490 (2012).

[5] W. Shangguan, Sci. Technol. Adv. Mater. **8**, 76 (2007).

[6] G. Chen, D. Li, F. Li, Y. Fan, H. Zhao, Y. Luo, R. Yu, Q. Menga, Appl. Catal. A **443– 444,** 138 (2012).

[7] L. Zheng, Y. Xu, Y. Song, C. Z. Wu, M. Zhang, Y. Xie, Inorganic Chemistry **48**, 4003 (2009).

[8] N. Z. Bao, L. M. Shen, T. Takata, K. Domen, Chem. Mater. **20**, 110 (2008).

[9] Z. B. Lei, W. S. You, M. Y. Liu, G. H. Zhou, T. Takata, M. Hara, K. Domen, C. Li, Chem. Commun. 2142 (2003).

[10] G. Chen, F. Li, Y. Fan, Y. Luo, D. Li, Q. Meng, Catal. Commun. **40**, 51 (2013).

[11] N. Biswal, D. P. Das, S. Martha, K. M. Parida, Int. J. Hydrogen Energy **36**, 13452 (2011).

[12] J. Wang, B. Li, J. Chen, N. Li, J. Zheng, J. Zhao, Z. Zhu, J. Alloys Compd. **535**, 15 (2002).

[13] A. Kudo, Y. Miseki, Chem. Soc. Rev. **38**, 253 (2009).

[14] M. Kitano, M. Hara, J. Mater. Chem. **20**, 627 (2010).

[15] A. Kudo, M. Sekizawa, Catal. Lett. **58**, 241 (1999).

[16] K. Zhang, D. Jing, C. Xing, L. Guo, Int. J. Hydrogen Energy **32,** 4685 (2007).

[17] S. Shen, L. Zhao, Z. Zhou, L. Guo, J. Phys. Chem. C **112**, 16148 (2008).

[18] G. Chen, Catal. Commun. **40**, 51 (2013).

[19] S. Hotchandani, P. V Kamat, J. Phys. Chem. **96**, 6834 (1992).

[20] Y. Wang, J. Wu, J. Zheng, R. Jiang, R. Xu, Catal. Sci. Technol. **2**, 581 (2012).

[21] X. Wang, G. Liu, G. Q. Lu, H. M. Cheng, Int. J. Hydrogen Energy **35,** 8199 (2010).

[22] B. Hu, Z. Jing, J. Huang, F. Jin, Optoelectron Adv. Mat. **8**, 282 (2014).

[23] Y. A. Kalandaragh, M. B. Muradov, R. K. Mamedov, M. Behboudnia, A. Khodayar, Optoelectron. Adv. Mat. **2**, 42 (2008).

[24] G. Raju,V. S. Kumar, M. Raja, J. Optoelectron. Adv. M. **15**(11-12), 1399 (2013).

[25] A. E. Morales, E. S. Mora, U. Pal, Rev. Mexicana Fís. **S53**, 18 (2007).

[26] R. Banica, T. Nyari, V. Sasca, Int. J. Hydrogen Energ. **37,** 16489 (2012).

[27] C. Zamfirescu, I. Dincer, G. F. Naterer, R. Banica, Chem. Eng. Sci. **97**, 235 (2013).

[28] P. Poulopoulos, B. Lewitz, A.Straub, S. D. Pappas, S. A. Droulias, S. Baskoutas, P. Fumagalli , Applied Physics Letters 100 , 211910 (2012);

[29] D. Kurbatov, A. Opanasyuk, S. Kshnyakina, V. Melnik, V. Nesprava, Rom. J. Phys. **55**, 213 (2010).

[30] N.K. Morozova, V.A. Kuznetsov, Zinc Sulfide Preparation and optical properties, Nauka, Moscow, (1987).

*Corresponding author: radu.banica@yahoo.com